Developments in the Built Environment 17 (2024) 100374

Contents lists available at ScienceDirect

Developments in the Built Environment

journal homepage: www.sciencedirect.com/journal/developments-in-the-built-environment

Water transport and porosity trends of concrete containing integral additions of raw-crushed wind-turbine blade

Víctor Revilla-Cuesta [a,b], Flora Faleschini [b], Carlo Pellegrino [b], Marta Skaf [c,*], Vanesa Ortega-López [a]

[a] Department of Civil Engineering, Escuela Politécnica Superior, University of Burgos, c/ Villadiego s/n, 09001, Burgos, Spain
[b] Department of Civil, Environmental and Architectural Engineering, University of Padova, via Francesco Marzolo 9, 35131, Padova, Italy
[c] Department of Construction, Escuela Politécnica Superior, University of Burgos, c/ Villadiego s/n, 09001, Burgos, Spain

ARTICLE INFO

Keywords:
Raw-crushed wind-turbine blade
Porous balsa wood
Concrete
Water absorption
Effective porosity
Porosity-based strength estimation

ABSTRACT

Raw-Crushed Wind-Turbine Blade (RCWTB) is a novel material from the recycling and non-selective crushing of wind-turbine blades composed of fiberglass-composite fibers and polyurethane and balsa-wood particles. This research evaluates for the first time the water-transport and porosity behaviors of concrete with RCWTB through water-penetration-under-pressure, full-immersion water-absorption, capillarity-water-absorption and mercury-intrusion-porosimetry tests. RCWTB contents of 1.5%, 3.0%, 4.5%, and 6.0% were considered. All the RCWTB concretes yielded adequate results for depth of water penetration under pressure and water-absorption rate, although this waste slightly worsened both properties. RCWTB also increased the proportion of pores between 100 and 250 nm in size, which increased total and capillary effective porosities to maximum values of 13.54% and 13.51%, respectively, and sharply decreased the compression-related mechanical properties of concrete. Capillary effective porosity included the porosity effect of balsa-wood particles on concrete mechanical performance, so it allowed estimating the compression-related mechanical properties with a deviation lower than ±10%.

1. Introduction

Concrete is a composite material consisting of cement, aggregate, and water, and very frequently admixtures. A fifth component, air, must be added to those four standard ingredients, as it is retained in small bubbles within the concrete mass during mixing (Urakov, 2022). Concrete is therefore a porous material, even though it may not appear so once it has set. In fact, porosity is a key property that should be controlled when designing any concrete mix, as it conditions both concrete durability (Cantero et al., 2021) and mechanical behavior (Revilla-Cuesta et al., 2021).

- On the one hand, concrete with higher porosity levels has more pathways for the entry of aggressive external agents (Cantero et al., 2022). Those agents can therefore corrode the reinforcements and damage the microstructure of the concrete (Santamaría et al., 2018), which progressively deteriorates after exposure to seasonal climatic cycles and environmental events (Faleschini et al., 2015).
- On the other hand, increased porosity also implies a weakening of both the cementitious matrix and the aggregate-matrix interfacial transition zones (Revilla-Cuesta et al., 2022). So, the main virtue of concrete for construction purposes, its mechanical strength, especially its compressive strength, is usually worse at higher porosity levels (Vu et al., 2022).

Concrete porosity can be measured in different ways. A first option is to use traditional methods based on the evaluation of the water-absorption capacity of concrete specimens, under either total immersion or exposed to the capillary action of water (Cantero et al., 2020). However, those tests only measure the effective porosity, *i.e.*, the volume of accessible pores that take in water (Villagrán Zaccardi et al., 2017). A second, more recent possibility is the use of X-ray computed tomography or micro-tomography, which consists of scanning concrete specimens through X-rays, detecting the pores, thanks to the lower density of the air than the surrounding concrete matrix (Vicente et al., 2021). However, one drawback of this technology is the need for high-power

* Corresponding author.
E-mail address: mskaf@ubu.es (M. Skaf).

https://doi.org/10.1016/j.dibe.2024.100374
Received 14 December 2023; Received in revised form 5 February 2024; Accepted 15 February 2024
Available online 22 February 2024

equipment to detect the smallest nanometer-sized pores (smaller 50 nm in size) (Chica et al., 2022). The most accurate option for the evaluation of concrete porosity is therefore Mercury Intrusion Porosimetry (MIP), which allows the detection of pores up to around 5 nm in size (Sidiq et al., 2020). This technique consists of testing pressurized mercury intrusion into a concrete sample weighing 2–3 g (Santamaría et al., 2020). The volume of intruded mercury yields both a measure of concrete porosity and pore-size distribution (Massana et al., 2018).

The relevance of porosity for concrete performance and the wide availability of porosity tests is reflected in numerous studies on concrete porosity and its effects on mechanical and durability performance (Abhilash et al., 2021; Moore et al., 2021; Nodehi et al., 2022). These studies have been widened following the recovery of what are generally wastes and industrial by-products and their conversion into alternative binders and aggregates for use in concrete (Bhagat and Savoikar, 2022; Cao et al., 2022; Rashad, 2022). Each alternative raw material has its own specific interactions within the concrete matrix and with the other components of the concrete mix, thereby altering the porosity patterns.

- The addition of alternative aggregates, slag aggregate and recycled concrete aggregate as the main exponents, modifies the porosity patterns of concrete, fundamentally due to their interaction with water and the necessary modification of the water/cement ratio (Rashad, 2022; Wu et al., 2022). Their higher water absorption compared to natural aggregate implies an increase in the water/cement ratio of concrete (Revilla-Cuesta et al., 2021), which leads to higher concrete porosity levels, due to the delayed evaporation of larger amounts of water (Rahman et al., 2016). Moreover, the use of the finer fractions of these aggregates usually implies higher porosity in the interfacial transition zones (Sivamani and Renganathan, 2022).
- The effect of binders on concrete porosity mainly depends on their physical characteristics. For example, total porosity is not modified, due to the higher fineness of ground granulated blast furnace slag compared to ordinary Portland cement, although higher proportions of smaller pores result in better durability and lower shrinkage (Weng and Liao, 2021). Another example is densified silica fume that, if not homogeneously distributed throughout the concrete mass after a faulty mixing process, will increase concrete porosity (Olek et al., 1990; Pedro et al., 2018).

Nevertheless, it is not only the use of these raw materials that affects concrete porosity. The addition of fibers is, for example, an adequate alternative to improve the bending-tensile behavior of concrete (Yavuz Bayraktar et al., 2023), although they can increase porosity when generating additional interfacial transition zones that disrupt the continuity of the cementitious matrix (Tran et al., 2022). Furthermore, the water content and, therefore, the water/cement ratio, usually have to be augmented when fibers are added to preserve concrete workability, which once again also increases porosity (Ortega-López et al., 2022). The interaction of each fiber type with all the other concrete components differs, as does the water content that is required whenever added to maintain workability (Camille et al., 2021; Xie et al., 2021; Zhang, X. et al., 2022; Muthukumarana et al., 2023). There are as a result numerous investigations on fiber types and their effects on concrete porosity (Ortega-López et al., 2022; Tran et al., 2022). These studies include research on recycled and natural fibers, in which the use of fibers within concrete is validated, thereby contributing to greener fiber-reinforced concrete (Liew and Akbar, 2020; Ahmad and Zhou, 2022; Tran et al., 2022).

The recycling of wind-turbine blades is currently a wind-power sector priority (Rani et al., 2021). The growing number of wind turbines to be dismantled over the coming years is driving the search for an inexpensive solution that will also add value to the dismantled blades (Fonte and Xydis, 2021). The varied composition of the blades, based on Glass Fiber-Reinforced Polymer (GFRP) composite, balsa wood, polyurethane and gel coatings complicates the search for a solution (Joustra et al., 2021). A line of research developed in very recent years has been on the mechanical treatment of the wind-turbine blades, either by machining or by crushing, so as to use the resulting product as a raw material in concrete (Yazdanbakhsh et al., 2018; Baturkin et al., 2021). The mechanical performance of concretes containing that raw material as aggregate is not suitable, regardless of whether the different blade components are separated prior to the mechanical treatment (Yazdanbakhsh et al., 2018; Baturkin et al., 2021; Pławecka et al., 2021). Nevertheless, GFRP-composite fibers, obtained after the mechanical processing of wind-turbine blade GFRP composite, have been successfully used in the production of fiber-reinforced concrete (Tao et al., 2023) and are now a valuable option for improving the bending-tensile behavior and load-bearing capacity of concrete (Yazdanbakhsh et al., 2018; Wei and Hadigheh, 2023). Good results have been reported both for the exclusive use of GFRP-composite fibers (Xu et al., 2022) and, if the blade components remain unseparated from the balsa wood and the polyurethane both before and after mechanical processing (Baturkin et al., 2021; Revilla-Cuesta et al., 2023). Therefore, according to the above-mentioned points regarding the use of wastes and fibers in concrete production, the addition of the waste material derived from the mechanical treatment of wind-turbine blades to concrete can alter its porosity patterns, due to the presence of both GFRP-composite fibers and particles of balsa wood and polyurethane (Zhang, Z. et al., 2022; Fernando et al., 2023). These particles serve as lightweight aggregate in the concrete mass, thereby adding physical characteristics quite unlike those of conventional natural aggregate (Jang and Kang, 2022).

Raw-Crushed Wind-Turbine Blade (RCWTB) is obtained by crushing wind-turbine blades with no prior separation of their components. This waste material is composed of GFRP-composite fibers and approximately spherical particles of balsa wood and polyurethane (Revilla-Cuesta et al., 2023). Therefore, the use of this material not only modifies the mechanical behavior of concrete due to the stitching effect of the fibers, but it also alters the porosity patterns of concrete. Concrete mixes containing integral additions of 0.0%, 1.5%, 3.0%, 4.5%, and 6.0% RCWTB are studied in this research, whose porosity levels are evaluated through conventional water-absorption techniques and MIP tests. The aim is to gain a better understanding of the effect of RCWTB on concrete porosity and the relationship between porosity and the mechanical behavior of concrete when this alternative material is used. The ultimate goal is to determine whether the use of RCWTB for the production of concrete is adequate in terms of porosity, an aspect that has yet to be resolved in the scientific literature.

2. Materials and methods

2.1. Raw materials

2.1.1. Conventional raw materials

The concrete mixes were prepared with conventional raw materials. CEM II/A-L 42.5 R as *per* EN 197–1 (EN-Euronorm) was used, with between 6% and 20% wt. Of limestone; tap water; two plasticizers to reduce the water content of the concrete, and that allow improving strength while maintaining workability according to previous experience (Fiol et al., 2018); and three sizes (0/2 mm, 2/6 mm, and 6/22 mm) of crushed siliceous aggregate. Their granulometry, detailed in Fig. 1a, was continuous and suitable for concrete manufacturing, and their density and water absorption levels, both with standard values, are shown in Table 1.

2.1.2. Raw-crushed wind-turbine blade (RCWTB)

RCWTB, as its name suggests, consists of crushed wind-turbine blade in raw form, *i.e.*, with no separation of its components (Joustra et al., 2021), that has been processed in a knife mill. The material resulting from the crushing was sieved, to ensure that all the components passed through a 10-mm-aperture sieve, and any material that was retained

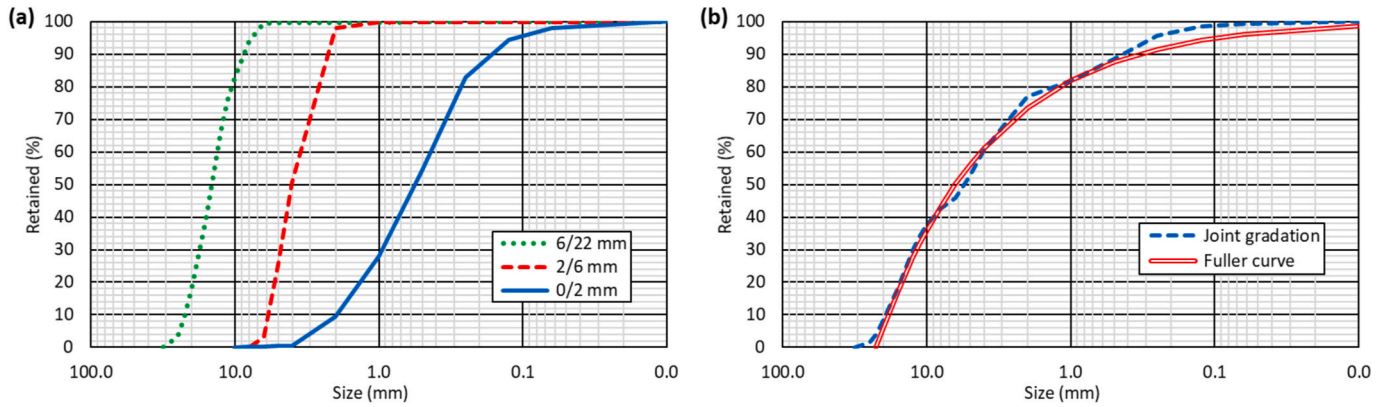

Fig. 1. Particle gradation: (a) aggregates; (b) concrete mixes.

Table 1
Density and water absorption as *per* EN 1097–6 (EN-Euronorm) of siliceous aggregate.

Fraction (mm)	6/22	2/6	0/2
Saturated-surface-dry density (kg/dm^3)	2.59	2.58	2.62
24-h water absorption (% wt.)	1.66	1.83	0.52

underwent a second crushing. All the characteristics of RCWTB, included an in-depth analysis through scanning electron microscopy, can be found elsewhere (Revilla-Cuesta et al., 2023). As a short summary, the RCWTB in the aforementioned study had an overall density of 1.63 kg/dm^3 and consisted of.

- GFRP-composite fibers (Fig. 2a), which represented 66.8 ± 3.1% wt. Of RCWTB. With an average length of 13.1 mm, the fibers increased the tensile strength of the concrete, and added post-cracking resistance (Rani et al., 2021).
- Balsa-wood particles (Fig. 2b), which represented 6.3 ± 0.2% wt. Of RCWTB. These particles presented an approximately spherical but slightly angular shape. Balsa wood served as a lightweight aggregate when RCWTB was added to concrete, its main characteristic being its low density (0.33 kg/dm^3). Accordingly, the balsa wood present in the RCWTB was of high density (Jang and Kang, 2022), with porosity levels between 70% and 75%, indicating that large amounts of water could be absorbed (Jang and Kang, 2022).
- Polyurethane particles (Fig. 2c), which approximately represented 8.3 ± 0.3% wt. Of RCWTB. Their shape was similar to the balsa-wood particles, their size was always under 10 mm, and they served as aggregate in concrete mixes (Bhagat and Savoikar, 2022).
- Micro-fibers and small non-separable particles (Fig. 2d), which represented 18.6 ± 0.5% wt. Of RCWTB. This fraction included glass fibers that had detached from the epoxy matrix of the GFRP composite, epoxy-resin powder, and small particles of balsa wood and polyurethane that were "entangled" within the glass fibers and could not be mechanically separated. Thus, its different respective components served as fibers and aggregates upon the incorporation of RCWTB within the concrete.

2.2. Mix design

The objective of the mix design was to reach an S3 slump class, as

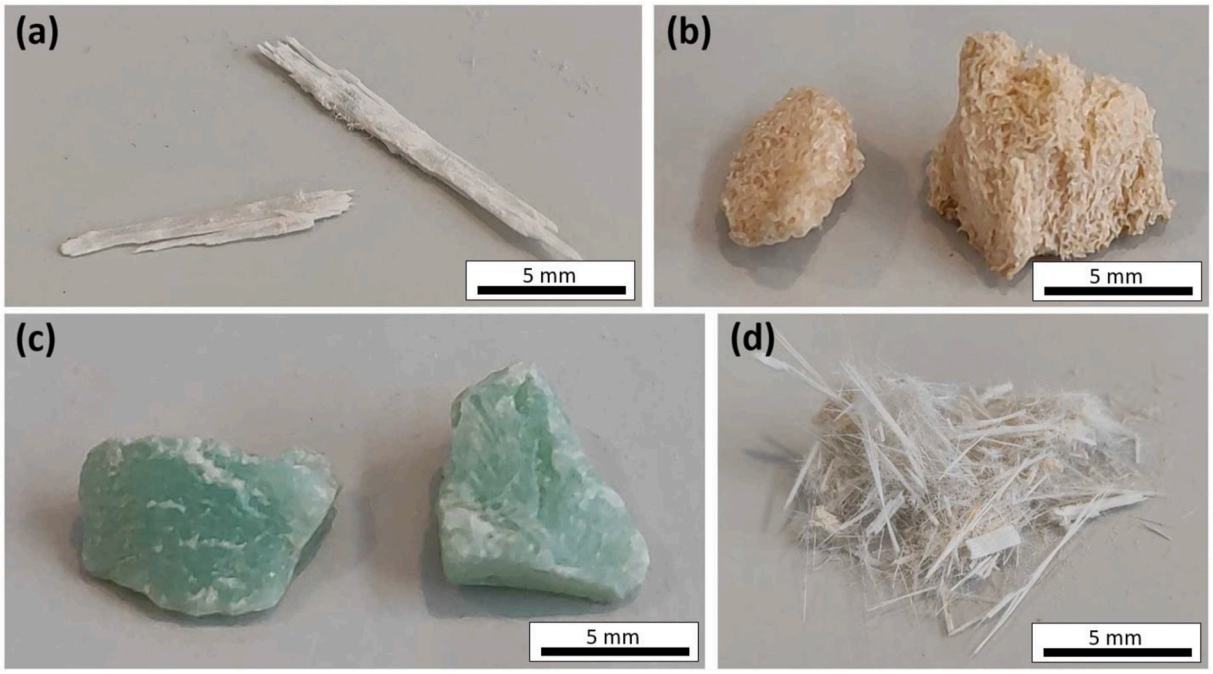

Fig. 2. Components of RCWTB: (a) GFRP-composite fibers; (b) balsa-wood particles; (c) polyurethane particles; (d) micro-fibers and small non-separable particles.

specified in EN 206 (EN-Euronorm), *i.e.*, a slump value of 12.5 ± 2.5 cm, for each of the five RCWTB additions (0.0%, 1.5%, 3.0%, 4.5%, and 6.0% by volume of the concrete mix) under consideration. In this way, any effects of concrete workability on the results would be similar (Forero et al., 2022).

The reference concrete (*M0.0* mix) was based on the design proportions of Eurocode 2 (EC-2, 2010), so as to ensure a minimum compressive strength of 45 MPa, which is valid for almost any use (EC-2, 2010). The proportion of each aggregate fraction was established looking for an optimum adjustment to the Fuller curve, the result being shown in Fig. 1b. The content of water and plasticizers then underwent small empirical modifications, before the final dosage shown in Table 2 was obtained.

Subsequently, integral additions of 1.5%, 3.0%, 4.5%, and 6.0% RCWTB by volume (mixes *M1.5*, *M3.0*, *M4.5*, and *M6.0*) were all separately added, while increasing the plasticizer and water contents at ratios of 10.55% and 0.93% *per* 1% RCWTB, to ensure the same slump class (Revilla-Cuesta et al., 2023). The primary objective of adding RCWTB was so that the fibers could improve the compressive strength performance of concrete, although the balsa wood and polyurethane particles serving as concrete aggregates also influenced its behavior.

2.3. Mixing process

The five-stage mixing process, detailed below and in Fig. 3, ensured a homogeneous distribution of all the concrete components and maximized workability (Revilla-Cuesta et al., 2023).

1. Separation of total water content into two parts before mixing: water for admixtures (0.5 L) and water for mixing (remainder of water in each mix).
2. Addition of the aggregates and 30% of the water for mixing, and mixing for 3 min.
3. Addition of cement and 70% of the total water for mixing, and mixing for 3 min.
4. Addition of half of the plasticizers diluted in 50% of the water for admixtures, and mixing for 2 min.
5. Addition of RCWTB, and mixing for 2 min.
6. Addition of the other half of the plasticizers diluted in 50% of the water for admixtures, and mixing for 5 min.

2.4. Experimental plan

After concrete mixing, the slump and air content were measured in the fresh state as *per* the instructions of EN 12350–2 (EN-Euronorm) and EN 12350–7 (EN-Euronorm), respectively, to provide an overview of the fresh performance of the concrete mixes. Subsequently, specimens were prepared for the hardened tests, which intended to characterize the mechanical performance and porosity of concrete. Three specimens were used for each test. All the specimens were stored in a humid chamber at a temperature of 20 ± 2 °C and a humidity level of 90 ± 5% until the start of each test.

Table 2
Comparative mix design (kg).

Mix	Cement	Water	Plasticizer 1 # Plasticizer 2	Aggregate (6/22 # 2/6 # 0/2)	RCWTB
M0.0	320	128	2.20 # 1.10	900 # 600 # 500	0.0
M1.5	320	133	2.62 # 1.31	900 # 600 # 500	24.5
M3.0	320	137	3.04 # 1.52	900 # 600 # 500	49.0
M4.5	320	142	3.46 # 1.73	900 # 600 # 500	73.5
M6.0	320	146	3.88 # 1.94	900 # 600 # 500	98.0

The composition of the *M0.0* reference mix corresponded to a volume of 1 m^3, a lower volume than in the mixes with RCWTB additions.

2.4.1. Mechanical tests

All dimensions of the mechanical performance of concrete were evaluated through the tests depicted in Table 3. These tests were performed at an age of 28 days, which is the standardized age for analyzing the mechanical behavior of concrete (EC-2, 2010).

2.4.2. Porosity tests

Tests were also performed to determine the porosity of concrete and analyze its relationship with the mechanical behavior (Revilla-Cuesta et al., 2021). All of them were conducted when the concrete was 90 days old to ensure that the long-term hydration of the cementitious matrix of the concrete was complete, so that this aspect no longer affected porosity (Fiol et al., 2023). The porosity evaluation of the concrete mixes was conducted through water-absorption and Mercury Intrusion Porosimetry (MIP) tests.

- The depth of water penetration under pressure was determined on 10 × 20-cm cylindrical specimens through the procedure specified in EN 12390–8 (EN-Euronorm). Thus, the skin was first removed from the lower circular face of the specimens, and then water was applied to the face at a pressure of 500 ± 50 kPa for 72 ± 2 h. After that time, the specimens were split open in the Brazilian splitting test, to measure the maximum and the average water-penetration depths.
- The full-immersion water absorption of concrete was measured according to UNE, 2014, and ASTM C642, 2013 on 10 × 10 × 10-cm cubic specimens. Therefore, the specimens were first conditioned in terms of humidity as *per* UNE, 2008a. Subsequently, they were progressively immersed in water, at a rate of one third of the specimen height *per* day to favor air expulsion. When they were completely submerged, the specimens were kept under these conditions until their mass stabilized. The specimens were weighed daily throughout the whole test.
- The capillary-water-absorption test was conducted as *per* UNE, 2008b and ASTM C1585, 2013 on 10 × 10 × 10-cm cubic specimens. This test began with the removal of the skin from the bottom face, opposite the concreting face, of the specimens. Then, after 24 h of conditioning of the specimens in moisture terms according to UNE, 2008a, the four lateral faces of the specimens were waterproofed to prevent any further water evaporation. The upper face, *i.e.*, the concreting face, was not waterproofed, so that the air could be expelled as the water entered. 24 h after waterproofing, the bottom face of each specimen, without its skin, was placed in contact with a 2-mm-thick water layer, so that the water penetrated the concrete by capillary action. The amount of water absorbed by the specimens over time was determined by weighing, initially quite frequently and then temporarily spaced out as the test progressed, until saturation.
- The MIP tests were performed at 90 days on 3-g internal fragments of cementitious matrix that contained balsa-wood and polyurethane particles that were imperceptible to the naked eye. The main objective was to evaluate only the porosity of the matrix (Chica et al., 2022). Those fragments were obtained from the specimens tested to compressive strength at 28 days and were kept in a moist room until an age of 90 days to obtain porosity results fully comparable with those of the other tests. After oven drying the fragments, the test was conducted using an AutoPore IV 9500 that applied a gradual increase of pressure between 0 and 30,000 psia and, therefore, an increase of mercury penetration within the concrete fragments.

2.5. Calculation of water-absorption rate and effective porosity

The capillary water absorption of concrete is usually analyzed using two models dependent on the square root of time: the Fangerlund model (UNE, 2008b) and Hall's model (Hall, 1989). Using both models, it is possible to calculate a coefficient that quantifies the water-absorption rate.

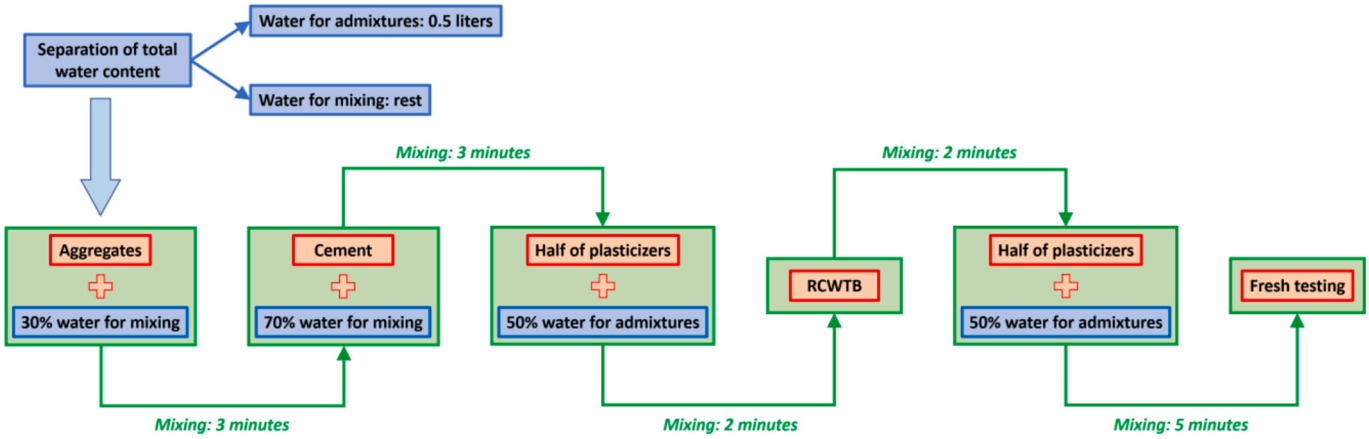

Fig. 3. Mixing process.

Table 3
Mechanical tests.

Test	Standard (EN-Euronorm)	Specimens
Hardened density	EN 12390-7	10 × 10 × 10-cm cubic specimens
Compressive strength	EN 12390-3	10 × 20-cm cylindrical specimens
Modulus of elasticity	EN 12390-13	10 × 20-cm cylindrical specimens
Splitting tensile strength	EN 12390-6	10 × 20-cm cylindrical specimens
Flexural strength	EN 12390-5	7.5 × 7.5 × 27.5-cm prismatic specimens

- On the one hand, there is the permeation coefficient, K, of the Fangerlund model (Equation (1)), which assumes a constant rate of water absorption from the beginning of the test up until concrete saturation. Thus, this coefficient is calculated by dividing the increase in mass of the concrete until saturation, ΔM, by the square root of the time of the process, $\Delta\sqrt{t}$.

$$K = \frac{\Delta M}{\Delta\sqrt{t}} \tag{1}$$

- On the other hand, there is the sorptivity, S, of the Hall's model, which represents the overall water-absorption rate of the concrete. It is calculated by fitting the model (Equation (2)) to the experimental results through a simple least-squares regression, in which ΔM is the mass increment and t is the time. A and B are simply regression-adjustment coefficients to model the performance of materials with coarse pore structures (Hall, 1989), such as concrete.

$$\Delta M = A + S \times \sqrt{t} - B \times t \tag{2}$$

Furthermore, if the increase in mass, ΔM, of a concrete as a consequence of capillary water absorption is known, then the effective porosity, ε_e, of the concrete can also be calculated, *i.e.*, the porosity formed by the interconnected pores accessible to water (Santamaría et al., 2018), through Equation (3), correcting for water density, ρ, and considering the volume of the specimen that is tested, V.

$$\varepsilon_e = \frac{\Delta M}{V \times \rho} \times 100 \tag{3}$$

All these models can also be applied to the full-immersion water-absorption test, as the temporal evolution of the concrete mass under these conditions is almost identical to that found in the capillary-water-absorption test (Cantero et al., 2020; Ortega-López et al., 2022).

3. Results and discussion

3.1. Physical-mechanical properties

The test results of both the fresh and the 28-day mechanical tests are shown in Table 4. As had been expected, the addition of RCWTB modified all the properties evaluated in the concrete mixes. A more detailed analysis of these concrete mixes and their fresh and mechanical properties can be found in another paper of the authors (Revilla-Cuesta et al., 2024).

Regarding the fresh properties, the increase in RCWTB content had no negative effects on the slump of the concrete, and even slightly increased it up to a maximum of 3 cm by adjusting the water and plasticizer content. Thus, all the mixes showed an S3 slump class as *per* EN 206 (EN-Euronorm). However, RCWTB had a negative effect on air content for three reasons. First, the RCWTB fibers favored the retention of air within the concrete, as with conventional fibers (Alsaif and Alharbi, 2022). Second, balsa wood promoted air retention, due to its high porosity (Jang and Kang, 2022). Finally, the content of water and admixtures was higher when adding RCWTB.

The hardened density of concrete was reduced with increasing RCWTB contents, due to the low overall density of RCWTB additions and the increased the water/cement ratios to maintain workability, which led to higher porosity levels (Islam et al., 2022).

The higher RCWTB content worsened compressive behavior, due to the higher water content (Ortega-López et al., 2022) and the interfacial transition zones containing balsa-wood and polyurethane particles were weaker than those containing natural aggregate (Al-Mansour et al., 2022). Both aspects could also lead to an increase in porosity that weakened both the cementitious matrix and the interfacial transition zones (Cantero et al., 2020). In addition, the fibers were unable to provide high strength under this type of stress (Muthukumarana et al., 2023). The splitting tensile strength remained approximately constant up to a RCWTB content of 3.0%, due to the stitching action of the GFRP-composite fibers (Ahmed et al., 2021). Higher contents of this waste weakened the cementitious-matrix bond, partially due to

Table 4
Average values of physical-mechanical properties.

Mix	*M0.0*	*M1.5*	*M3.0*	*M4.5*	*M6.0*
Slump (cm)	10.0	10.5	13.0	13.5	12.0
Air content (% vol.)	1.8	2.0	2.0	2.2	2.6
Density (kg/dm^3)	2.40	2.35	2.33	2.28	2.27
Compressive strength (MPa)	52.5	52.5	47.5	40.4	41.8
Modulus of elasticity (GPa)	41.0	37.8	34.2	27.8	29.4
Splitting tensile strength (MPa)	3.97	4.03	3.94	3.44	3.35
Flexural strength (MPa)	6.05	5.93	5.75	5.89	6.06

increased porosity in the interfacial transition zones (Revilla-Cuesta et al., 2021), so much so that the fibers were unable to compensate for that negative effect (Ortega-López et al., 2021), thereby decreasing the splitting tensile strength by 0.5–0.6 MPa in the *M4.5* and *M6.0* mixes. Finally, the flexural strength decreased in the *M1.5* and *M3.0* mixes due to their weaker compressive behavior (Islam et al., 2022). At higher waste contents, the proportion of GFRP-composite fibers within the concrete was sufficient for them to exercise a stitching effect that effectively increased the strength in the tensile zone, resulting in increased flexural strength (Ahmed et al., 2021). Thus, concrete porosity was less relevant in this mechanical property, so the *M0.0* and *M6.0* mixes had approximately the same flexural strength, at around 6.0 MPa.

3.2. Depth of water penetration under pressure

The maximum and the average water-penetration depths obtained in the water-penetration-under-pressure test are shown in Fig. 4. Although no precise evaluation of concrete porosity emerged from this test, it provided a first approach to mix behavior in terms of durability (Cantero et al., 2021; Ortega-López et al., 2022).

Both the maximum and average penetration depths increased with the integral additions of RCWTB to the concrete, following the same trend as the air content (Table 4). Thus, the addition of RCWTB undoubtedly resulted in higher porosity levels, which is thought to be mainly due to three aspects. First, the presence of fibers, which created additional interfacial transition zones that disrupted the continuity of the cementitious matrix (Vicente et al., 2021), apart from increasing the porosity, because of the necessary adjustment of the water/cement ratio when added (Ortega-López et al., 2022). Secondly, the presence of polyurethane particles with weaker and more porous bonding within the cementitious matrix than the natural-aggregate particles (Islam et al., 2022). Finally, the presence of balsa-wood particles, which were able to absorb water due to their high porosity (Jang and Kang, 2022).

The maximum penetration depth increased approximately linearly with the RCWTB content up to 3.0% waste (32.4% increase for the *M3.0* mix), after which it remained almost constant. This behavior may have been due to the barrier effect of the GFRP-composite fibers, which limited the water penetration under pressure for high RCWTB contents (Liew and Akbar, 2020). However, the average penetration depth increased steadily with the RCWTB content, at 91.8% for the *M6.0* mix. The use of RCWTB was therefore more negative in terms of average water-penetration depth, which might be due to the overall content of water that penetrated within the concrete was more evenly distributed as a result of the fibers and the particles of balsa wood and polyurethane.

Nevertheless, all the mixes would be valid for use in any class of environmental exposure both in terms of maximum depth (less than 30 mm) and average depth (less than 20 mm), as *per* the international standards (EC-2, 2010). The results showed that producing concrete with high contents of RCWTB is a suitable option as long as an adequate mix design is conducted that meets the water-penetration-under-pressure requirements found in international standards (EC-2, 2010).

3.3. Full-immersion water absorption

The full-immersion water-absorption test was performed to evaluate the water-absorption capacity and porosity of the concrete samples completely submerged in water (Santamaría et al., 2018). These conditions hindered the expulsion of the air occupying the pores within the concrete, with the result that the measured porosity was generally lower than the true value (Cantero et al., 2021). In addition, if the porosity resulting from this test is compared with the total porosity, then the sealing effect of the concrete skin can be evaluated (Baltazar et al., 2014).

The average evolution of the mass of each concrete mix over the full-immersion water-absorption test is shown in Fig. 5. From an overall perspective, water absorption exhibited a growing tendency with increasing RCWTB contents, existing a positive linear correlation of 0.84 between them. Thus, the mass of the *M0.0*-mix specimens had increased 34.0 g at the end of the test, while that same increase for the *M6.0* mix was 44.1 g (29.6% increase). As might be guessed from the results of the water-penetration-under-pressure test, the use of this waste material undoubtedly increased the water absorption capacity of the concrete as a consequence not only of the higher porosity of the cementitious matrix (Pławecka et al., 2021), but also of the presence of particles of balsa wood, with a high porosity (Fig. 2b) (Jang and Kang, 2022). However, there were two exceptions to this general behavior.

- On average, the *M1.5* mix absorbed less water than the reference mix (31.2 g vs. 34.0 g). This result showed that the use of small RCWTB additions may be beneficial in this particular concrete behavior. It appears that the GFRP-composite fibers exerted a barrier effect on the intake of water (Li et al., 2022), which compensated for the other negative porosity-related effects.
- The *M4.5* mix showed a higher increase in mass than the *M6.0* mix (48.5 g vs. 44.1 g). The influence of the increased RCWTB content on the water absorption of concrete stabilized at a content of 4.5%. As was the case with the *M1.5* mix, the fibers favored slightly less water absorption that might have compensated for the effects of both

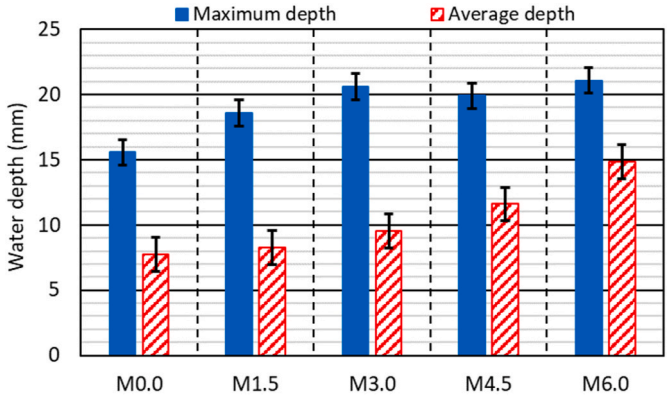

Variation due to RCWTB addition (%) regarding the *M0.0* mix					
Depth	***M0.0***	***M1.5***	***M3.0***	***M4.5***	***M6.0***
Maximum	0.0	19.5	32.4	27.9	35.5
Average	0.0	7.1	23.2	50.0	91.8

Fig. 4. Depth of water penetration under pressure.

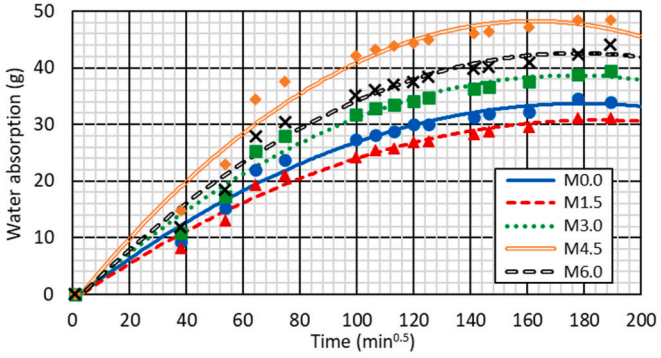

Mix	Fangerlund	Hall (depicted in the graph)				Effective porosity (% vol.)
	K (g/min$^{0.5}$)	*A* (g)	*S* (g/min$^{0.5}$)	*B* (g/min)	R^2 (%)	
M0.0	0.274	-1.0239	0.3872	0.0011	98.21	3.40
M1.5	0.242	-1.0522	0.3426	0.0009	98.39	3.12
M3.0	0.318	-1.2846	0.4527	0.0013	98.09	3.95
M4.5	0.421	-1.6971	0.6161	0.0019	97.45	4.85
M6.0	0.352	-1.5032	0.4965	0.0014	97.90	4.41

Fig. 5. Water absorption and porosity by full immersion.

increased porosity and the accumulation of water within the balsa-wood particles (Liew and Akbar, 2020).

3.3.1. Water-absorption-rate coefficients

The values of both the permeation coefficient and the sorptivity obtained in the full-immersion water-absorption test are shown in Fig. 5. The use of RCWTB not only increased the amount of water absorbed after full immersion of the concrete, but its addition also led the concrete to absorb the water more quickly. Therefore, higher water-absorption-rate coefficients were obtained when adding higher amounts of RCWTB. Absorbed-water mass and water-absorption rate were therefore directly proportional. The exceptions were the behavior of the *M1.5* and *M6.0* mixes. The *M1.5* mix had a lower water-absorption rate than the *M0.0* reference mix because the barrier effect of the GFRP-composite fibers to water flow caused by 1.5% RCWTB was more noticeable than the increased porosity that this RCWTB amount caused. For a RCWTB content of 6%, the content of GFRP-composite fibers was high enough to compensate for the increased porosity when adding this waste, which created effective barriers to water penetration within the concrete mass. This resulted in the water-absorption rate of the *M6.0* mix being lower than that of the *M4.5* mix.

The permeation coefficient and the sorptivity levels of the mixes were between 0.25 and 0.45 g/min$^{0.5}$ and between 0.35 and 0.60 g/min$^{0.5}$, respectively. As usual, the sorptivity values were higher, because Hall's model is a global approach to the whole water absorption process, not only the initial part (Cantero et al., 2021; Revilla-Cuesta et al., 2021). Finally, two other aspects can be highlighted in relation to Hall's model, which are also noted in Fig. 5. On the one hand, its results projected a very accurate fit with the temporal evolution of water absorption, with R^2 coefficients above 97%, despite the fact that this test was performed under full-immersion conditions. On the other hand, the mixes with large additions of RCWTB (the *M4.5* and the *M6.0* mixes) reached saturation levels earlier on, shown with a very clear maximum point in Hall's model (Hall, 1989).

3.3.2. Effective porosity

The results of effective porosity obtained from the full-immersion water-absorption test are shown in Fig. 5, which are in line with the aspects discussed for this test. Thus, the effective porosity of the reference mix was 3.40%; the *M1.5* mix, 3.12%; the *M4.5* mix, 4.85%; and the *M6.0* mix, 4.41%. These porosity results showed once again the effectiveness of GFRP-composite fibers in acting as a barrier to water flow when RCWTB was added in 1.5% and 6.0% contents.

The values of porosity obtained in this test were small compared to the usual porosity levels of concrete (Santamaría et al., 2020), as detailed in subsequent sections. The reason was because all mixes, regardless of RCWTB content, showed effective opposition to water ingress under full immersion, due to the difficulty of expelling air within the concrete matrix and the skin-sealing effect (Ortega-López et al., 2022). Finally, it can be noted that the increase in the water-absorption rate was linked to the increase in the effective porosity, as it increased the number of pathways for water to enter within the concrete (Cantero et al., 2021).

3.4. Capillary water absorption

The evolution of specimen mass of the different concrete mixes over the capillary-water-absorption test, as well as their permeation coefficients, *K*, (Equation (1)), their sorptivities, *S*, (Equation (2)), and their effective porosities, ε_e, (Equation (3)) are detailed in Fig. 6.

The temporal evolution of the mass of the concrete mixes followed the same trend as obtained in the full-immersion water-absorption test. Thus, the increase in RCWTB content in general led to higher capillary water absorption, due to the increase in the porosity of the cementitious matrix, because of the appearance of new interfacial transition zones

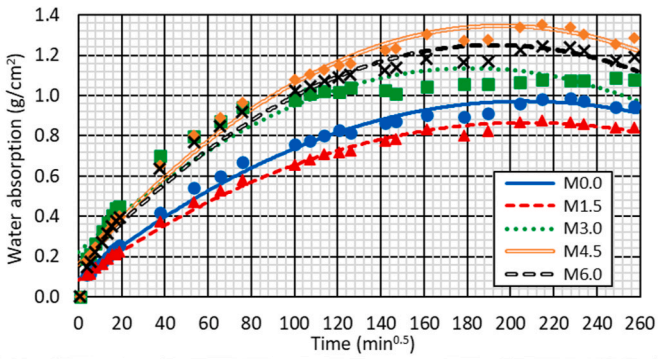

Mix	Fangerlund	Hall (depicted in the graph)				Effective porosity (% vol.)
	K (g/min$^{0.5}$)	*A* (g)	*S* (g/min$^{0.5}$)	*B* (g/min)	R^2 (%)	
M0.0	0.5944	8.7380	0.8565	0.0021	99.05	9.87
M1.5	0.5444	8.3137	0.7531	0.1018	99.28	8.79
M3.0	0.7225	22.1574	1.0055	0.0027	94.76	10.87
M4.5	0.8627	15.9240	1.2120	0.0031	98.76	13.51
M6.0	0.7937	15.2746	1.1397	0.0030	98.23	12.46

Fig. 6. Water absorption and porosity by capillarity.

following the introduction of fibers and polyurethane particles within the concrete (Liew and Akbar, 2020; Islam et al., 2022), as well as the increase of the water/cement ratio to maintain constant workability (Ortega-López et al., 2022). Moreover, the presence of balsa-wood particles also increased capillary water absorption, not only because of their weaker interfacial transition zones, but also because of their high porosity and water-absorption levels (Jang and Kang, 2022). Thus, the balsa-wood particles served both as aggregates and as water accumulation points within the concrete. As in the full-immersion water-absorption test, the water absorption levels of the *M1.5* mix and the *M6.0* mix were lower than the reference mix *M0.0* and the *M4.5* mix, respectively. In both cases, it is thought that the fibers in RCWTB served as barriers to water flow (Li et al., 2022). In the *M1.5* mix, this effect was perceptible, due to the low content of polyurethane and balsa-wood particles within the concrete, while in the *M6.0* mix, it is suggested that the higher content of GFRP-composite fibers could have had a beneficial effect.

Similar trends in terms of mass increase caused the water-absorption-rate coefficients and effective porosity to follow the same trends.

- Both the permeation coefficient, *K*, and sorptivity, *S*, increased when adding RCWTB, leading to faster capillary water absorption, due to the increased porosity, and the presence of porous balsa-wood particles (Revilla-Cuesta et al., 2021; Wang et al., 2021). Again, the exceptions were the *M1.5* and *M6.0* mixes. On the other hand, the sorptivity of the mixes was 0.3 g/min$^{0.5}$ higher than the permeation coefficient, due to its calculation throughout the entire water-absorption process rather than the initial part (Hall, 1989). Finally, the permeation coefficient of all the mixtures corresponded to good-quality concrete, with values below 0.90 g/min$^{0.5}$ (Metha and Monteiro, 2014).
- The effective porosity of the mixes also increased with RCWTB content. Effective porosity measured not only the accessible porosity of the cementitious matrix itself (Cantero et al., 2022), but also the accessible porosity of the balsa-wood particles, which was also occupied by water (Wang et al., 2021). It is thought that the high porosity of the balsa wood was the cause of such a sharp increase in porosity, as it was 36.9% higher in the *M4.5* mix than in the *M0.0* mix. The effective porosity values of the mixes corresponded to values qualified as good at around or slightly lower than 12% (Metha and Monteiro, 2014). The effective porosity of the *M4.5* mix could be classified as habitual (Metha and Monteiro, 2014).

3.4.1. Approach through the fourth root of time

As can be noted in Fig. 6, the initial evolution of the mass of the concrete specimens, due to capillary water absorption as a function of the square root of time, was not linear. In addition, the fit of Hall's model showed that the specimens of all the mixes reached theoretical saturation before complete weight stabilization (see maximum points in Fig. 6) (Hall, 1989). Both aspects are very common when alternative raw materials are used for concrete production, and sometimes hinder the accurate definition of the capillary water-absorption rate of concrete (Cantero et al., 2021; Revilla-Cuesta et al., 2021). This situation has led to the development of alternative approaches to describe the capillary water-absorption behavior of concrete, which try to establish a linear relationship between the capillary water absorption of concrete and the independent variable that is chosen. One widely accepted approach is to express the increase of concrete mass caused by capillary water absorption as a function of the fourth root of time, performing an adjusted linear regression under those conditions (Villagrán Zaccardi et al., 2017). In this case, sorptivity is the slope of the straight line that is obtained. This approach is usually quite accurate and easy to apply (Villagrán Zaccardi et al., 2017), reasons for which it was selected for the RCWTB concrete mixes of this study. The results of this approximation are shown in Fig. 7.

The capillary water-absorption model as a function of the fourth root of time fitted the mixes with RCWTB more accurately than conventional models such as Hall's model (Fig. 7), in all cases presenting R^2 coefficients higher than 97.50%. In fact, the sorptivities of the Hall's model and this alternative model showed the same trends, increasing with the addition of larger amounts of RCWTB, except in the *M1.5* and *M6.0* mixes, due presumedly to the barrier effect of the fibers against water flow (Li et al., 2022). The sorptivity values in this case were between 6 and 10 g/min$^{0.25}$.

3.4.2. Comparison of full-immersion and capillarity tests

The comparison of the water-absorption-rate coefficients and effective porosity obtained in the full-immersion water-absorption and capillary water-absorption tests is shown in Table 5. The values obtained under full-immersion conditions were lower than under capillary water absorption conditions, due to the difficulty of expelling air and the sealing effect of the concrete skin when the specimens were completely immersed in water (Cantero et al., 2022). However, it can be noted that the ratio between the results of both tests was almost the same for all the mixes. Thus, the two water-absorption-rate coefficients were approximately 2.2 times higher under capillary conditions than under full immersion, as the 95%-confidence intervals show in Table 5. Similarly, the effective porosity was 2.8 times higher. Results that point to the quality of the concrete skin that the additions of RCWTB left unaffected. The skin hindered water ingress in the same relative terms for all mixes. Even though the removal of the skin manifests an increase in porosity as a result of the RCWTB additions, the skin of the concrete continued to be equally effective at hindering the entry of water and harmful external agents within the concrete (Pedro et al., 2018; Santamaría et al., 2018).

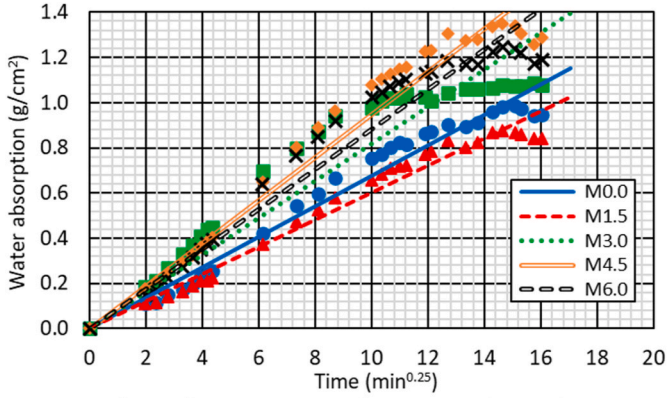

Mix	*S* (g/(cm²·min$^{0.25}$))	*S* (g/min$^{0.25}$)	R^2 (%)
M0.0	0.0676	6.76	99.29
M1.5	0.0603	6.03	99.34
M3.0	0.0818	8.18	97.63
M4.5	0.0949	9.49	98.98
M6.0	0.0884	8.84	98.81

Fig. 7. Capillary water absorption as a function of the fourth root of time.

Table 5
Capillarity results vs. full-immersion results.

Mix	Permeation coefficient *K*	Sorptivity *S*	Effective porosity
M0.0	2.17	2.21	2.90
M1.5	2.25	2.20	2.82
M3.0	2.27	2.22	2.75
M4.5	2.05	1.97	2.79
M6.0	2.25	2.30	2.83
95%-confidence interval	2.198 ± 0.113	2.179 ± 0.154	2.818 ± 0.069

Results of the capillary-water-absorption test divided by the results of the full-immersion water-absorption test.

3.5. Mercury Intrusion Porosimetry (MIP)

The numerical results of the MIP tests are listed in Table 6, while the log differential and cumulative intrusions for the five concrete mixes are plotted in Fig. 8.

As shown in the second row of Table 6, and consistent with the results of the water-absorption tests, the total porosity of the mixes, in this case exclusively measured in the cementitious matrix, increased with the addition of RCWTB, with the exceptions of the *M1.5* and *M6.0* mixes. Maximum total porosity was observed in the *M4.5* mix, with a value of 13.54%, an increase in porosity although not necessarily implying a larger total pore area (third row of Table 6), possibly due to the increase in the proportion of larger-diameter pores apart from the total porosity (Ortega-López et al., 2022). Nevertheless, increased porosity in general led to an increase in the mean pore size (fourth row of Table 6), from 88.9 nm in the *M0.0* mix, to 111.4 nm in the *M6.0* mix (25.3% increase). Thus, the results of total pore area and median pore diameter were coherent with each other (Sidiq et al., 2020). Finally, as the hardened-density test had revealed (Table 4), the addition of RCWTB reduced concrete density (fifth row of Table 6), in this case due to the increased porosity it caused (Bhagat and Savoikar, 2022). These reductions were 1.6% in the *M3.0* mix and 5.1% in the *M6.0* mix.

Pore-size distributions in terms of log differential (Fig. 8a) and cumulative intrusions (Fig. 8b) were similar in all the mixes, and they all showed conventional pore-size distributions for a cement-based material (Santamaría et al., 2020). Thus, the intrusion slowly increased with decreasing pore size until reaching a pore diameter of 100–200 nm, from which it started to increase much faster (Fig. 8b). Additions of RCWTB increased cementitious-matrix porosity, without notably changing the log differential intrusion indices, as all of the indices showed similar intrusion peaks at pore diameters of 80–90 nm. The only relevant differences between the mixes were the peaks of the *M6.0* mix and, especially, the *M4.5* mix in relation to a pore size of 200 nm (Fig. 8a). That increase in pore-size proportion could have been the cause of the sharper

Table 6
Numerical results of the MIP tests.

Mix	*M0.0*	*M1.5*	*M3.0*	*M4.5*	*M6.0*
Total porosity (%)	10.65	9.77	11.80	13.54	12.59
Total pore area (m²/g)	3.00	3.39	3.96	3.86	3.90
Median pore diameter (nm)	88.9	73.5	88.8	103.8	111.4
Density (kg/dm³)	2.55	2.53	2.51	2.43	2.42

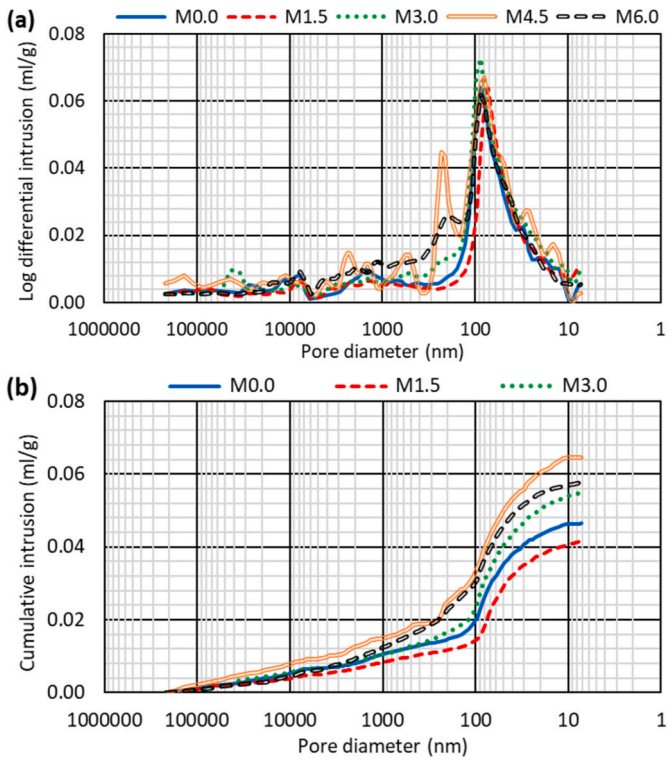

Fig. 8. Graphical results of the MIP tests: (a) log differential intrusion; (b) cumulative intrusion.

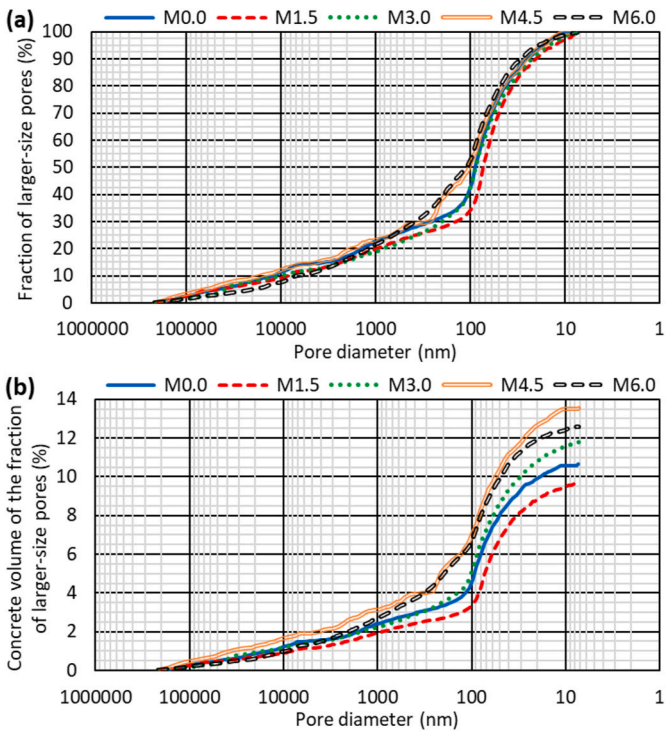

Fig. 9. MIP results for pore-size distribution in terms of: (a) total porosity; (b) concrete volume.

decrease in all mechanical properties (Table 4), except for flexural strength that was strongly conditioned by the presence of fibers in the RCWTB (Xu et al., 2022). Nevertheless, it is a hypothesis that needs further verification through studying the overall pore-size distributions and MIP effective-porosity levels.

3.5.1. *Overall pore-size distributions and MIP effective porosity*

The overall pore-size-distribution curves were obtained from the total-porosity values and the pore-size-distribution curves of the MIP tests (Sidiq et al., 2020). Those results are represented in percentages of total porosity (assuming that the total porosity is 100%) in Fig. 9a and refer to total concrete volume in Fig. 9b. Those curves show that all the mixes initially presented a smooth increase in the percentage of pores with decreasing pore size until a specific pore diameter was reached, followed by a sharper increase.

- For mixtures with RCWTB contents equal to or less than 3.0%, this pore size was approximately 100 nm. Thus, larger pore sizes accounted for approximately 35–40% of the total porosity (3.5–4.5% of total concrete volume).
- The *M4.5* and *M6.0* mixes also experienced an abrupt change in the rate at which porosity increased at around 200–250 nm. Approximately 30% of the pores in the cementitious matrix of both mixes were oversized (4% of the concrete volume), in similar proportions to those of the other mixes. Nevertheless, 50% of the pores were larger than 100 nm in size (7% of the concrete volume) in the *M4.5* and *M6.0* mixes. A result that shows that both RCWTB contents not only increased the porosity of the concrete, but also increased the proportion of larger pore sizes (between 100 and 250 nm) (Sidiq et al., 2020). These large pore sizes might also be favored by the increased proportion of water and plasticizer with the addition of RCWTB at those levels (Santamaría et al., 2020; Cantero et al., 2022).

Pores smaller than 70 nm have practically no effect on the water-transport behavior and the mechanical properties of the concrete samples (Metha and Monteiro, 2014). Thus, the concept of effective porosity can be defined in terms of the MIP test, which is the porosity formed by pores larger than 70 nm (Metha and Monteiro, 2014). The effective MIP porosity of each mixture is detailed in Table 7. Each value was obtained by multiplying the total porosity by the percentages of pores larger than 70 nm, which were around 60–70% of the total porosity in all the mixes, except for the *M1.5* mix, with around 50% (Fig. 9a). These values corroborated the hypothesis that the *M4.5* and *M6.0* mixes presented a higher proportion of pores larger than 70 nm (between 100 and 250 nm according to Fig. 9), as there was a much more pronounced increase in the effective MIP porosity (increase of 9.9% for the *M3.0* mix and 36.2% for the *M4.5* mix). According to the literature, that behavior is linked to a worsening of the mechanical properties (Ortega-López et al., 2022; Vu et al., 2022), as may be noted in the mixes of this study, shown in Table 4. The presence of RCWTB fibers compensated for this worsening of cementitious-matrix quality in terms of flexural strength (Liew and Akbar, 2020; Ahmed et al., 2021).

3.5.2. *MIP results comparison*

According to the previous discussions, the MIP tests provided values of density and effective porosity for each concrete mix. These results can be compared with those obtained in the hardened-density and capillary water-absorption tests.

The density values, both in specimens and through MIP, showed that the higher the RCWTB content, the lower the concrete density. However, the cause of the density decrease in both tests was different. The decrease in density when the specimens were tested was because of the increased porosity of the concrete with additions of RCWTB (Tran et al., 2022), and the presence of balsa-wood and polyurethane particles that

Table 7
Effective MIP porosity.

Mix	*M0.0*	*M1.5*	*M3.0*	*M4.5*	*M6.0*
Total porosity (%)	10.65	9.77	11.80	13.54	12.59
Effective MIP porosity (%)	6.66	4.98	7.32	9.07	8.69

acted as aggregates and presented a much lower density than the natural-aggregate particles (Islam et al., 2022; Jang and Kang, 2022). However, in the MIP test, the test fragments incorporated no balsa-wood nor polyurethane particles visible to the naked eye and the density decrease was solely and exclusively due to the increase in porosity (Chica et al., 2022). Thus, the MIP density was always higher than the specimen-testing density (Ortega-López et al., 2022). However, the quotient of the MIP density and specimen test results were very similar for all the mixes, presenting a value between 1.06 and 1.08, more specifically 1.071 ± 0.012, calculated with a 95%-confidence interval (Fig. 10). However, it can be observed that the MIP density was closer to the specimen-testing density in the *M4.5* and *M6.0* mixes. The higher proportion of balsa wood and polyurethane within those mixtures may have caused some very small particles of these materials to be present in the MIP analyses of the fragments, which might have further reduced the MIP density result (Wang et al., 2021).

The comparison of the porosities obtained in the MIP and the capillary-water-absorption tests is shown in Fig. 11. As can be seen in Fig. 9a, the effective MIP porosity (porosity including only pores with a diameter greater than 70 nm (Metha and Monteiro, 2014)) was approximately between 60% and 70% of the total porosity. These values of effective MIP porosity were approximately 30% lower than those of capillary effective porosity in absolute terms, including the *M0.0* reference mix. Therefore, the water absorbed by capillarity occupied pores within the cementitious matrix with a size less than 70 nm (Santamaría et al., 2020). The results also showed that as the RCWTB content increased, the value of the capillary effective porosity edged closed to the total MIP porosity (ratio of 0.927 in the *M0.0* mix and 0.990 in the *M6.0* mix). The capillary effective porosity included the porosity of the balsa-wood particles, which were also saturated with water in the test (Jang and Kang, 2022), an aspect that was ignored in the total MIP porosity test. It resulted in virtual equality between the capillary effective porosity and the total MIP porosity for the *M4.5* and *M6.0* mixes. In the concrete incorporating RCWTB, it appeared that the effective porosity measured by concrete capillarity was very similar to the total MIP porosity of the cementitious matrix, disregarding the effect of the balsa wood.

3.6. Relationship between porosity and mechanical properties

Porosity significantly conditions not only the durability of concrete (Cantero et al., 2022; Cao et al., 2022), but also its mechanical behavior as its increase causes a weakening of the cementitious matrix (Wu et al., 2022). In the literature, there are numerous approaches and models that

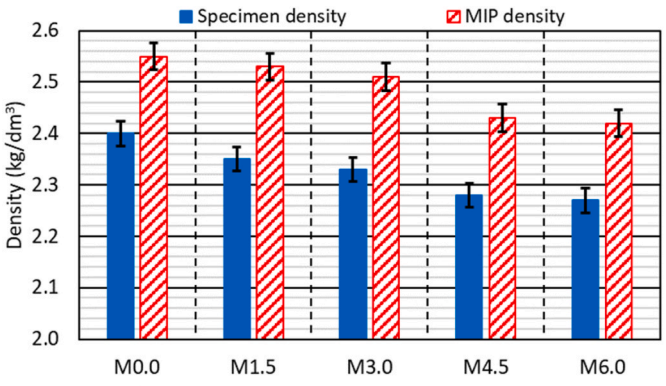

Ratio of MIP density to specimen density				
M0.0	***M1.5***	***M3.0***	***M4.5***	***M6.0***
1.063	1.077	1.077	1.066	1.066
95%-confidence interval			1.071±0.012	

Fig. 10. Comparison of concrete density determined by specimen testing and by MIP.

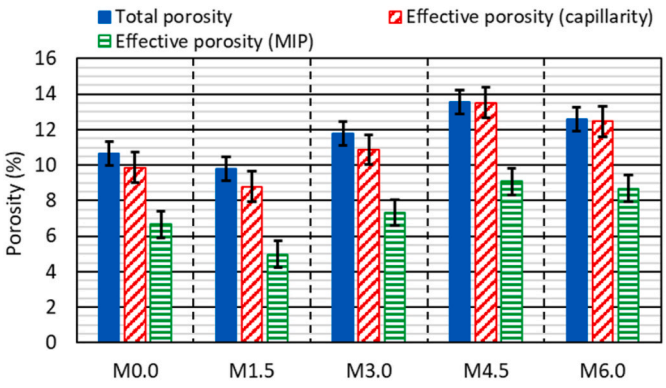

Ratio of effective porosity to total porosity					
Effective porosity through	***M0.0***	***M1.5***	***M3.0***	***M4.5***	***M6.0***
Capillarity	0.927	0.900	0.921	0.998	0.990
MIP	0.625	0.510	0.620	0.670	0.690

Fig. 11. Comparison of total and effective porosities.

are used to explain the mechanical behavior of concrete in terms of its porosity (Kurihashi et al., 2020; Blasone et al., 2021; Revilla-Cuesta et al., 2021). It is such a relevant aspect that it should be analyzed in concrete containing RCWTB, to find an adequate explanation for its behavior. Table 8 shows the simple-regression models with the best fit for each 28-day mechanical property (compressive strength, modulus of elasticity, splitting tensile strength, and flexural strength), as a function of each porosity type (total porosity, capillary effective porosity, and effective MIP porosity). The following aspects can be derived from this statistical analysis.

- The best-fit model was different for each mechanical property, due to the different influence of RCWTB and porosity for each one. However, the best-fit model was the same for all three porosity types, which shows that all the porosity types followed the same trends (Revilla-Cuesta et al., 2021).
- The simple-regression fit was good for compressive-behavior-related properties (R^2 coefficients greater than 90% for compressive strength and greater than 80% for modulus of elasticity) and acceptable for splitting tensile strength (R^2 coefficient only greater than 75%). However, the fit was very poor for flexural strength. Results that indicate that porosity is not a valid variable to explain the evolution of flexural strength when adding RCWTB, due to the presence of fibers that stitch the cementitious matrix and increase the strength in the tensile zone (Xie et al., 2021; Xu et al., 2022). In the rest of the properties, GFRP-composite fibers played a less relevant role, porosity being a key factor to explain mechanical performance.
- Finally, the best fit (higher R^2 coefficients) for all mechanical properties was obtained with capillary effective porosity. As mentioned above, the porosity included the effect of balsa-wood particles, which absorbed water due to their high porosity (Wang et al., 2021). The presence of those particles affected the mechanical behavior of concrete, because of their weaker bond with the cementitious matrix than the natural aggregate (Baturkin et al., 2021). Thus, the porosity that included this aspect was the one that best explained the mechanical behavior of the concrete.

The regression models of the mechanical properties as a function of porosity are shown in Fig. 12. The inadequate fit of flexural strength can be appreciated, although the capillary effective porosity value was satisfactorily used to estimate the values of the other mechanical properties to a maximum deviation of ±10%.

Table 8
Best-fitting simple-regression adjustment models of the mechanical properties as a function of porosity.

Mechanical property	Best-adjustment model	Total porosity			Effective porosity through capillarity			Effective porosity through MIP		
		a	*b*	R^2	*a*	*b*	R^2	*a*	*b*	R^2
Compressive strength	$y = (a - b \times x^2)^2$	8.443	0.012	93.33	8.051	0.010	95.20	7.804	0.017	91.29
Modulus of elasticity	$y = {}^{1}/_{(a + b \times x^2)}$	0.012	0.00013	87.09	0.016	0.00011	89.55	0.019	0.00019	81.05
Splitting tensile strength	$y = \sqrt{a - b \times x^2}$	22.351	0.060	76.45	20.596	0.051	84.67	19.386	0.094	84.62
Flexural strength	$y = {}^{1}\Big/\left(a - b_{/x}\right)$	0.172	0.044	1.86	0.169	0.009	0.15	0.168	0.001	0.19

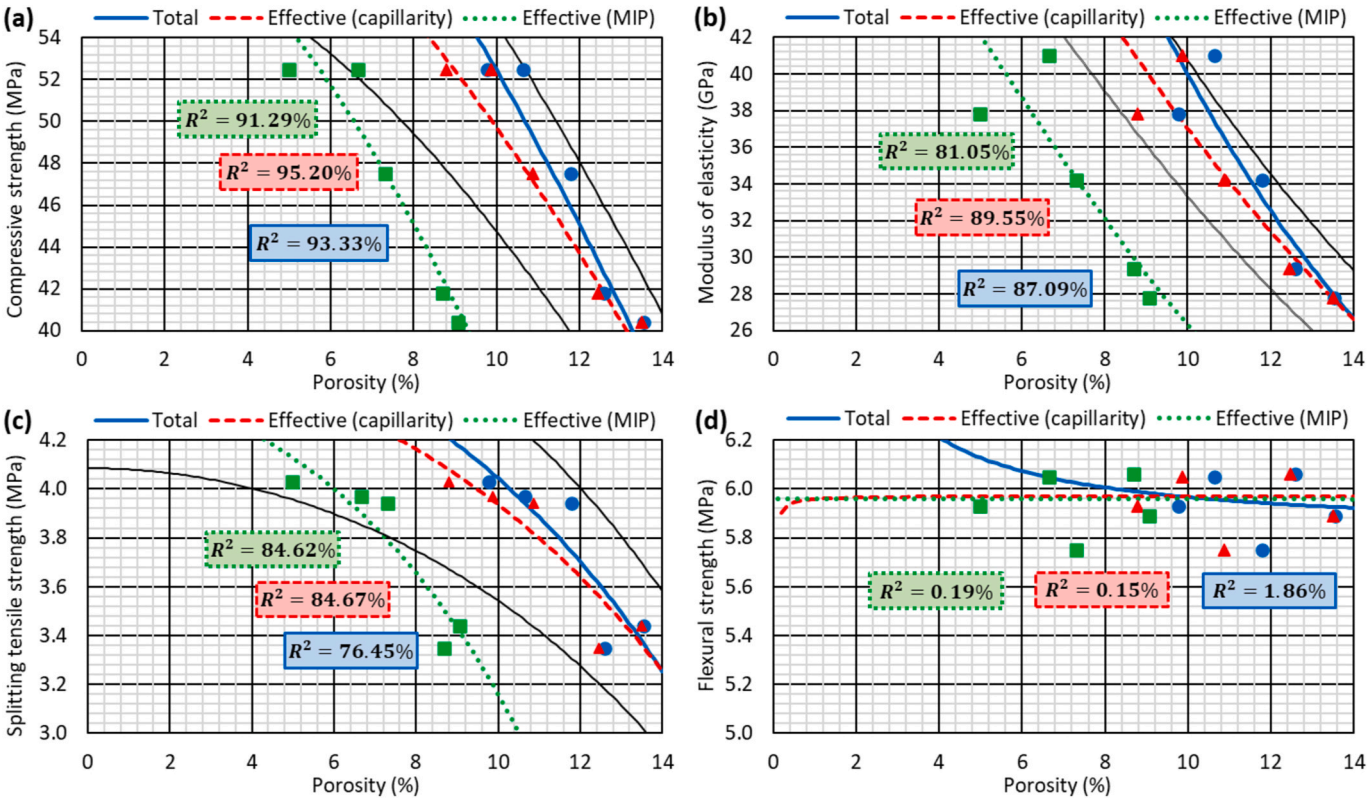

Fig. 12. Mechanical properties as a function of porosity: (a) compressive strength; (b) modulus of elasticity; (c) splitting tensile strength; (d) flexural strength. Black continuous lines represent the limits of the ±10% prediction deviation for the capillary-effective-porosity model.

4. Conclusions

The water-transport performance and porosity of concrete mixes made with 0.0%, 1.5%, 3.0%, 4.5%, and 6.0% Raw-Crushed Wind-Turbine Blade (RCWTB) have been studied in this paper. This waste material was composed of fibers from the crushing of Glass Fiber-Reinforced Polymer (GFRP) composite, and particles of balsa wood and polyurethane. Specimens of all mixtures were tested for depth of water penetration under pressure, full-immersion water absorption, and capillary water absorption. In addition, Mercury Intrusion Porosimetry (MIP) tests were used to determine the porosity of cementitious-matrix fragments. The following conclusions can be drawn from all the aspects discussed.

- RCWTB addition increased both the maximum and average depths of water penetration. Even so, all the values met the limits for concrete use under the most unfavorable environmental conditions.
- RCWTB increased the water-absorption levels of the concrete, both under full-immersion and capillary-action conditions. However, both small (1.5% RCWTB) and large amounts (6.0% RCWTB) never increased water absorption as much as the mixes with 0.0% and 4.5% RCWTB, respectively. GFRP-composite fibers could effectively act as barriers against water flow for those RCWTB amounts.
- The higher the RCWTB content, the higher the water-absorption rate of the concrete specimens, although the values obtained were in all cases indicative of a good-quality concrete. The consideration of the fourth power of time provided linearity when computing this property.
- RCWTB increased concrete porosity. Furthermore, RCWTB contents of 4.5% and 6.0% augmented the proportion of pores with a size between 100 and 250 nm according to MIP tests, which caused a noticeable decrease of the mechanical properties less influenced by the RCWTB fibers.
- The sealing effect of the concrete skin was the same regardless of the RCWTB content according to the effective porosities measured by full immersion. In turn, capillary effective porosity was very similar to total MIP porosity, which accounted only the porosity of the cementitious matrices and not the high porosity of the balsa-wood particles within the RCWTB.
- The compressive strength, modulus of elasticity and splitting tensile strength of the RCWTB concrete could be estimated through porosity with a maximum deviation of ±10%. The flexural strength depended

on the stitching effect of RCWTB fibers, being porosity less relevant. Capillary effective porosity provided the most accurate estimation, as it accounted for the balsa-wood effect.

Overall, although the use of RCWTB led to an increase in the water absorption and porosity of concrete, it was found to be within the appropriate limits for use in all types of elements. However, the effect of balsa wood should also be lent special attention in future studies and when using this concrete type, in view of its high porosity and water-absorption levels.

CRediT authorship contribution statement

Víctor Revilla-Cuesta: Writing – original draft, Software, Methodology, Investigation, Formal analysis, Data curation, Conceptualization. **Flora Faleschini:** Writing – review & editing, Visualization, Supervision, Methodology, Data curation. **Carlo Pellegrino:** Writing – review & editing, Validation, Supervision, Methodology, Formal analysis. **Marta Skaf:** Writing – review & editing, Resources, Investigation, Funding acquisition, Formal analysis, Conceptualization. **Vanesa Ortega-López:** Writing – review & editing, Supervision, Software, Project administration, Funding acquisition, Conceptualization.

Declaration of competing interest

The authors declare that they have no known competing financial interests or personal relationships that could have appeared to influence the work reported in this paper.

Data availability

Data will be made available on request.

Acknowledgements

This research work was supported by the Spanish Ministry of Universities within the framework of the State Program for the Promotion of Talent and Employability in R + D + i, State Mobility Subprogram, of the State Plan for Scientific and Technical Research and Innovation 2021–2023 [CAS22/00013]; MICINN, AEI, EU, ERDF and NextGenerationEU/PRTR [grant numbers PID2020-113837RB-I00; PID2023-146642OB-I00; 10.13039/501100011033; TED2021-129715B–I00]; the Junta de Castilla y León (Regional Government) and ERDF [grant number UIC-231; BU033P23]; the University of Burgos [grant number SUCONS, Y135.GI]; and, finally, the University of Padova.

References

Abhilash, P.P., Nayak, D.K., Sangoju, B., Kumar, R., Kumar, V., 2021. Effect of nano-silica in concrete; a review. Construct. Build. Mater. 278, 122347 https://doi.org/10.1016/j.conbuildmat.2021.122347.

Ahmad, J., Zhou, Z., 2022. Mechanical properties of natural as well as synthetic fiber reinforced concrete: a review. Construct. Build. Mater. 333, 127353 https://doi.org/10.1016/j.conbuildmat.2022.127353.

Ahmed, H.U., Faraj, R.H., Hilal, N., Mohammed, A.A., Sherwani, A.F.H., 2021. Use of recycled fibers in concrete composites: a systematic comprehensive review. Composites, Part B 215, 108769. https://doi.org/10.1016/j.compositesb.2021.108769.

Al-Mansour, A., Chen, S., Xu, C., Peng, Y., Wang, J., Ruan, S., Zeng, Q., 2022. Sustainable cement mortar with recycled plastics enabled by the matrix-aggregate compatibility improvement. Construct. Build. Mater. 318, 125994 https://doi.org/10.1016/j.conbuildmat.2021.125994.

Alsaif, A., Alharbi, Y.R., 2022. Strength, durability and shrinkage behaviours of steel fiber reinforced rubberized concrete. Construct. Build. Mater. 345, 128295 https://doi.org/10.1016/j.conbuildmat.2022.128295.

ASTM C642, 2013. Standard Test Method for Density, Absorption, and Voids in Hardened Concrete.

ASTM C1585, 2013. Standard Test Method for Measurement of Rate of Absorption of Water by Hydraulic-Cement Concretes.

Baltazar, L., Santana, J., Lopes, B., Paula Rodrigues, M., Correia, J.R., 2014. Surface skin protection of concrete with silicate-based impregnations: influence of the substrate roughness and moisture. Construct. Build. Mater. 70, 191–200. https://doi.org/10.1016/j.conbuildmat.2014.07.071.

Baturkin, D., Hisseine, O.A., Masmoudi, R., Tagnit-Hamou, A., Massicotte, L., 2021. Valorization of recycled FRP materials from wind turbine blades in concrete. Resour. Conserv. Recycl. 174, 105807 https://doi.org/10.1016/j.resconrec.2021.105807.

Bhagat, G.V., Savoikar, P.P., 2022. Durability related properties of cement composites containing thermoplastic aggregates – a review. J. Build. Eng. 53, 104565 https://doi.org/10.1016/j.jobe.2022.104565.

Blasone, M., Saletti, D., Baroth, J., Forquin, P., Bonnet, E., Delaplace, A., 2021. Ultra-high performance fibre-reinforced concrete under impact of an AP projectile: parameter identification and numerical modelling using the DFHcoh-KST coupled model. Int. J. Impact Eng. 152, 103838 https://doi.org/10.1016/j.ijimpeng.2021.103838.

Camille, C., Kahagala Hewage, D., Mirza, O., Mashiri, F., Kirkland, B., Clarke, T., 2021. Performance behaviour of macro-synthetic fibre reinforced concrete subjected to static and dynamic loadings for sleeper applications. Construct. Build. Mater. 270, 121469 https://doi.org/10.1016/j.conbuildmat.2020.121469.

Cantero, B., Sáez del Bosque, I.F., Matías, A., Sánchez de Rojas, M.I., Medina, C., 2020. Water transport mechanisms in concretes bearing mixed recycled aggregates. Cem. Concr. Compos. 107, 103486 https://doi.org/10.1016/j.cemconcomp.2019.103486.

Cantero, B., Bravo, M., de Brito, J., Sáez del Bosque, I.F., Medina, C., 2021. Water transport and shrinkage in concrete made with ground recycled concrete-additioned cement and mixed recycled aggregate. Cem. Concr. Compos. 118, 103957 https://doi.org/10.1016/j.cemconcomp.2021.103957.

Cantero, B., Sáez del Bosque, I.F., Sánchez de Rojas, M.I., Matías, A., Medina, C., 2022. Durability of concretes bearing construction and demolition waste as cement and coarse aggregate substitutes. Cem. Concr. Compos. 134, 104722 https://doi.org/10.1016/j.cemconcomp.2022.104722.

Cao, Y., Bao, J., Zhang, P., Sun, Y., Cui, Y., 2022. A state-of-the-art review on the durability of seawater coral aggregate concrete exposed to marine environment. J. Build. Eng. 60, 105199 https://doi.org/10.1016/j.jobe.2022.105199.

Chica, L., Mera, C., Sepúlveda-Cano, L.M., Alzate, A., 2022. Porosity estimation and pore structure characterization of foamed cement paste using non-specialized image digital processing. Mater. Struct. 55 (7), 189. https://doi.org/10.1617/s11527-022-02031-6.

EC-2, 2010. Eurocode 2: Design of Concrete Structures. Part 1-1: General Rules and Rules for Buildings. CEN (European Committee for Standardization).

EN-Euronorm, Rue de stassart, 36. Belgium-1050 Brussels, European Committee for Standardization..

Faleschini, F., Alejandro Fernández-Ruíz, M., Zanini, M.A., Brunelli, K., Pellegrino, C., Hernández-Montes, E., 2015. High performance concrete with electric arc furnace slag as aggregate: mechanical and durability properties. Construct. Build. Mater. 101, 113–121. https://doi.org/10.1016/j.conbuildmat.2015.10.022.

Fernando, S., Gunasekara, C., Shahpasandi, A., Nguyen, K., Sofi, M., Setunge, S., Mendis, P., Rahman, M.T., 2023. Sustainable cement composite integrating waste cellulose fibre: a comprehensive review. Polymers 15 (3), 520. https://doi.org/10.3390/polym15030520.

Fiol, F., Thomas, C., Muñoz, C., Ortega-López, V., Manso, J.M., 2018. The influence of recycled aggregates from precast elements on the mechanical properties of structural self-compacting concrete. Construct. Build. Mater. 182, 309–323. https://doi.org/10.1016/j.conbuildmat.2018.06.132.

Fiol, F., Revilla-Cuesta, V., Thomas, C., Manso, J.M., 2023. Self-compacting concrete containing coarse recycled precast-concrete aggregate and its durability in marine-environment-related tests. Construct. Build. Mater. 377, 131084 https://doi.org/10.1016/j.conbuildmat.2023.131084.

Fonte, R., Xydis, G., 2021. Wind turbine blade recycling: an evaluation of the European market potential for recycled composite materials. J. Environ. Manag. 287, 112269 https://doi.org/10.1016/j.jenvman.2021.112269.

Forero, J.A., Bravo, M., Pacheco, J., de Brito, J., Evangelista, L., 2022. Thermal performance of concrete with reactive magnesium oxide as an alternative binder. Sustainability 14 (10), 5885. https://doi.org/10.3390/su14105885.

Hall, C., 1989. Water sorptivity of mortars and concretes: a review. Mag. Concr. Res. 41 (147), 51–61. https://doi.org/10.1680/macr.1989.41.147.51.

Islam, M.J., Shahjalal, M., Haque, N.M.A., 2022. Mechanical and durability properties of concrete with recycled polypropylene waste plastic as a partial replacement of coarse aggregate. J. Build. Eng. 54, 104597 https://doi.org/10.1016/j.jobe.2022.104597.

Jang, E.S., Kang, C.W., 2022. Porosity analysis of three types of balsa (Ochroma pyramidale) wood depending on density. J. Wood Sci. 68 (1), 31. https://doi.org/10.1186/s10086-022-02037-2.

Joustra, J., Flipsen, B., Balkenende, R., 2021. Structural reuse of wind turbine blades through segmentation. Composite. Part. C. Open Access 5, 100137. https://doi.org/10.1016/j.jcomc.2021.100137.

Kurihashi, Y., Kono, K., Komuro, M., 2020. Response characteristics of a steel fiber-reinforced porosity-free concrete beam under an impact load. Int. J. Civ. Eng. 18 (6), 673–684. https://doi.org/10.1007/s40999-020-00501-y.

Li, Z., Shen, A., Zeng, G., Chen, Z., Guo, Y., 2022. Research progress on properties of basalt fiber-reinforced cement concrete. Mater. Today Commun. 33, 104824 https://doi.org/10.1016/j.mtcomm.2022.104824.

Liew, K.M., Akbar, A., 2020. The recent progress of recycled steel fiber reinforced concrete. Construct. Build. Mater. 232, 117232 https://doi.org/10.1016/j.conbuildmat.2019.117232.

Massana, J., Reyes, E., Bernal, J., León, N., Sánchez-Espinosa, E., 2018. Influence of nano- and micro-silica additions on the durability of a high-performance self-compacting concrete. Construct. Build. Mater. 165, 93–103. https://doi.org/10.1016/j.conbuildmat.2017.12.100.

Metha, P.K., Monteiro, P.J.M., 2014. Concrete: Microstructure, Properties and Materials, fourth ed. 2014. McGraw-Hill Education. ISBN 978-0-07-179787-0.
Moore, A.J., Bakera, A.T., Alexander, M.G., 2021. A critical review of the Water Sorptivity Index (WSI) parameter for potential durability assessment: can WSI be considered in isolation of porosity? J. S. Afr. Inst. Civ. Eng. 63 (2), 27–34. https://doi.org/10.17159/2309-8775/2021/v63n2a4.
Muthukumarana, T.V., Arachchi, M.A.V.H.M., Somarathna, H.M.C.C., Raman, S.N., 2023. A review on the variation of mechanical properties of carbon fibre-reinforced concrete. Construct. Build. Mater. 366, 130173 https://doi.org/10.1016/j.conbuildmat.2022.130173.
Nodehi, M., Aguayo, F., Nodehi, S.E., Gholampour, A., Ozbakkaloglu, T., Gencel, O., 2022. Durability properties of 3D printed concrete (3DPC). Autom. ConStruct. 142, 104479 https://doi.org/10.1016/j.autcon.2022.104479.
Olek, J., Cohen, M.D., Lobo, C., 1990. Determination of surface area of portland cement and silica fume by mercury intrusion porosimetry. ACI Mater. J. 87 (5), 473–478.
Ortega-López, V., García-Llona, A., Revilla-Cuesta, V., Santamaría, A., San-José, J.T., 2021. Fiber-reinforcement and its effects on the mechanical properties of high-workability concretes manufactured with slag as aggregate and binder. J. Build. Eng. 43, 102548 https://doi.org/10.1016/j.jobe.2021.102548.
Ortega-López, V., Revilla-Cuesta, V., Santamaría, A., Orbe, A., Skaf, M., 2022. Microstructure and dimensional stability of slag-based high-workability concrete with steelmaking slag aggregate and fibers. J. Mater. Civ. Eng. 34 (9), 04022224 https://doi.org/10.1061/(ASCE)MT.1943-5533.0004372.
Pedro, D., de Brito, J., Evangelista, L., 2018. Durability performance of high-performance concrete made with recycled aggregates, fly ash and densified silica fume. Cem. Concr. Compos. 93, 63–74. https://doi.org/10.1016/j.cemconcomp.2018.07.002.
Pławecka, K., Przybyła, J., Korniejenko, K., Lin, W.T., Cheng, A., Łach, M., 2021. Recycling of mechanically ground wind turbine blades as filler in geopolymer composite. Materials 14 (21), 6539. https://doi.org/10.3390/ma14216539.
Rahman, S., Grasley, Z., Masad, E., Zollinger, D., Iyengar, S., Kogbara, R., 2016. Simulation of mass, linear momentum, and energy transport in concrete with varying moisture content during cooling to cryogenic temperatures. Transport Porous Media 112 (1), 139–166. https://doi.org/10.1007/s11242-016-0636-8.
Rani, M., Choudhary, P., Krishnan, V., Zafar, S., 2021. A review on recycling and reuse methods for carbon fiber/glass fiber composites waste from wind turbine blades. Composites, Part B 215, 108768. https://doi.org/10.1016/j.compositesb.2021.108768.
Rashad, A.M., 2022. Behavior of steel slag aggregate in mortar and concrete - a comprehensive overview. J. Build. Eng. 53, 104536 https://doi.org/10.1016/j.jobe.2022.104536.
Revilla-Cuesta, V., Faleschini, F., Zanini, M.A., Skaf, M., Ortega-López, V., 2021. Porosity-based models for estimating the mechanical properties of self-compacting concrete with coarse and fine recycled concrete aggregate. J. Build. Eng. 44, 103425 https://doi.org/10.1016/j.jobe.2021.103425.
Revilla-Cuesta, V., Skaf, M., Santamaría, A., Romera, J.M., Ortega-López, V., 2022. Elastic stiffness estimation of aggregate–ITZ system of concrete through matrix porosity and volumetric considerations: explanation and exemplification. Arch. Civ. Mech. Eng. 22 (2), 59. https://doi.org/10.1007/s43452-022-00382-z.
Revilla-Cuesta, V., Skaf, M., Ortega-López, V., Manso, J.M., 2023. Raw-crushed wind-turbine blade: waste characterization and suitability for use in concrete production. Resour. Conserv. Recycl. 198, 107160 https://doi.org/10.1016/j.resconrec.2023.107160.
Revilla-Cuesta, V., Manso-Morato, J., Hurtado-Alonso, N., Skaf, M., Ortega-López, V., 2024. Mechanical and environmental advantages of the revaluation of raw-crushed wind-turbine blades as a concrete component. J. Build. Eng. 82, 108383 https://doi.org/10.1016/j.jobe.2023.108383.
Santamaría, A., Orbe, A., San José, J.T., González, J.J., 2018. A study on the durability of structural concrete incorporating electric steelmaking slags. Construct. Build. Mater. 161, 94–111. https://doi.org/10.1016/j.conbuildmat.2017.11.121.
Santamaría, A., González, J.J., Losáñez, M.M., Skaf, M., Ortega-López, V., 2020. The design of self-compacting structural mortar containing steelmaking slags as aggregate. Cem. Concr. Compos. 111, 103627 https://doi.org/10.1016/j.cemconcomp.2020.103627.
Sidiq, A., Gravina, R.J., Setunge, S., Giustozzi, F., 2020. High-efficiency techniques and micro-structural parameters to evaluate concrete self-healing using X-ray tomography and Mercury Intrusion Porosimetry: a review. Construct. Build. Mater. 252, 119030 https://doi.org/10.1016/j.conbuildmat.2020.119030.
Sivamani, J., Renganathan, N.T., 2022. Effect of fine recycled aggregate on the strength and durability properties of concrete modified through two-stage mixing approach. Environ. Sci. Pollut. Res. 29 (57), 85869–85882. https://doi.org/10.1007/s11356-021-14420-5.
Tao, Y., Hadigheh, S.A., Wei, Y., 2023. Recycling of glass fibre reinforced polymer (GFRP) composite wastes in concrete: a critical review and cost benefit analysis. Structures 53, 1540–1556. https://doi.org/10.1016/j.istruc.2023.05.018.
Tran, N.P., Gunasekara, C., Law, D.W., Houshyar, S., Setunge, S., 2022. Microstructural characterisation of cementitious composite incorporating polymeric fibre: a comprehensive review. Construct. Build. Mater. 335, 127497 https://doi.org/10.1016/j.conbuildmat.2022.127497.
UNE83966, 2008a. Concrete Durability. Test Methods. Conditioning of Concrete Test Pieces for the Purpose of Gas Permeability and Capilar Suction Tests.
UNE83980, 2014. Concrete Durability. Test Methods. Determination of the Water Absorption, Density and Accesible Porosity for Water in Concrete.
UNE83982, 2008b. Concrete durability. Test methods. Determination of the capillar suction in hardened concrete. Fagerlund method.
Urakov, A.L., 2022. Review article: atmospheric pressure, water with air, porosity and strength of concrete (in memory of professor lászló A gömze). J. Phys. Conf. Ser. 2315, 012034 https://doi.org/10.1088/1742-6596/2315/1/012034.
Vicente, M.A., Mena, Á., Mínguez, J., González, D.C., 2021. Use of computed tomography scan technology to explore the porosity of concrete: scientific possibilities and technological limitations. Appl. Sci. 11 (18), 8699. https://doi.org/10.3390/app11188699.
Villagrán Zaccardi, Y.A., Alderete, N.M., De Belie, N., 2017. Improved model for capillary absorption in cementitious materials: progress over the fourth root of time. Cement Concr. Res. 100, 153–165. https://doi.org/10.1016/j.cemconres.2017.07.003.
Vu, V.H., Tran, B.V., Hoang, V.H., Nguyen, T.H.G., 2022. The effect of porosity on the elastic modulus and strength of pervious concrete. Lect. Notes Mech. Eng. 823–829. https://doi.org/10.1007/978-981-16-3239-6_63.
Wang, Z., Lin, S., Li, X., Zou, H., Zhuo, B., Ti, P., Yuan, Q., 2021. Optimization and absorption performance of wood sponge. J. Mater. Sci. 56 (14), 8479–8496. https://doi.org/10.1007/s10853-020-05547-w.
Wei, Y., Hadigheh, S.A., 2023. Development of an innovative hybrid thermo-chemical recycling method for CFRP waste recovery. Composites, Part B 260, 110786. https://doi.org/10.1016/j.compositesb.2023.110786.
Weng, J.R., Liao, W.C., 2021. Microstructure and shrinkage behavior of high-performance concrete containing supplementary cementitious materials. Construct. Build. Mater. 308, 125045 https://doi.org/10.1016/j.conbuildmat.2021.125045.
Wu, H., Wang, C., Ma, Z., 2022. Drying shrinkage, mechanical and transport properties of sustainable mortar with both recycled aggregate and powder from concrete waste. J. Build. Eng. 49, 104048 https://doi.org/10.1016/j.jobe.2022.104048.
Xie, J., Kou, S.C., Ma, H., Long, W.J., Wang, Y., Ye, T.H., 2021. Advances on properties of fiber reinforced recycled aggregate concrete: experiments and models. Construct. Build. Mater. 277, 122345 https://doi.org/10.1016/j.conbuildmat.2021.122345.
Xu, G.T., Liu, M.J., Xiang, Y., Fu, B., 2022. Valorization of macro fibers recycled from decommissioned turbine blades as discrete reinforcement in concrete. J. Clean. Prod. 379, 134550 https://doi.org/10.1016/j.jclepro.2022.134550.
Yavuz Bayraktar, O., Kaplan, G., Shi, J., Benli, A., Bodur, B., Turkoglu, M., 2023. The effect of steel fiber aspect-ratio and content on the fresh, flexural, and mechanical performance of concrete made with recycled fine aggregate. Construct. Build. Mater. 368, 130497 https://doi.org/10.1016/j.conbuildmat.2023.130497.
Yazdanbakhsh, A., Bank, L.C., Rieder, K.A., Tian, Y., Chen, C., 2018. Concrete with discrete slender elements from mechanically recycled wind turbine blades. Resour. Conserv. Recycl. 128, 11–21. https://doi.org/10.1016/j.resconrec.2017.08.005.
Zhang, X., Gao, X., Ding, Y., Xu, P., Zhou, G., Xu, J., 2022. Axial compression behavior of basalt fiber-reinforced recycled aggregate concrete-filled square steel tubular stub column. Struct. Concr. 23 (1), 365–381. https://doi.org/10.1002/suco.202100016.
Zhang, Z., Wong, Y.C., Sofi, M., Mendis, P., 2022. Incorporation of glass and plastic waste into alkali-activated mill residue bricks. Sustainability 14 (24), 16533. https://doi.org/10.3390/su142416533.